Supporting Information

Constructing Metallic Zinc-Cobalt Sulfide Hierarchical Core-Shell Nanosheet Arrays derived from 2D Metal-Organic-Framework for Flexible Asymmetric Supercapacitor with Ultrahigh Specific Capacitance and Performance†

Wei Sun,[a] Yuchuan Du,[b] Guangming Wu,[a] Guohua Gao,[a,*] Han Zhu,[c,*] Jun Shen,[a] Kun Zhang,[a] and Guozhong Cao[d,*]

[a]Shanghai Key Laboratory of Special Artificial Microstructure Materials and Technology School of Physics Science and Engineering, Tongji University, Shanghai 200092, China

[b]Key Laboratory of Road and Traffic Engineering (Ministry of Education), Tongji University, Shanghai 200092, China

[c]Key Laboratory of Synthetic and Biological Colloids (Ministry of Education), School of Chemical and Material Engineering, Jiangnan University, Wuxi 214122, China

[d]Department of Materials Science and Engineering, University of Washington Seattle, WA 98195, USA

*Corresponding authors: E-mail: gao@tongji.edu.cn (G. Gao), E-mail: zhuhanfj@163.com (H. Zhu), E-mail: gzcao@uw.edu (G. Cao).

Density functional theory calculation:

Density functional theory (DFT) computation was applied to investigate the crystal structural, elastic and electrical properties of ZnCoO, CoS and ZnCoS. All the calculations in this paper were performed using the Vienna *ab initio* simulation package (VASP).[1] The exchange-correlation energy was computed using the Perdew-Burke-Ernzerh functional of variant of the generalized gradient approximation (GGA).[2] Interaction between ion and electron was described with projector augmented wave pseudo potentials (PAW) approach,[3,4] and the energy cutoff for the plane wave basis set was set to be 400 eV. Based on the cubic Co_3O_4 and hexagonal CoS, a k-points sampling of $6\times6\times6$ and $15\times15\times3$ were employed for ZnCoO and ZnCoS, respectively, and the total energy was coverged to 10^{-5} eV.

For elasticity calculations, the formulas of elastic moduli and mechanical stability criteria will be firstly introduced for the considered crystal systems. The formulas of elastic moduli for cubic and hexagonal phase are based on Ref. 5 and Ref. 6,[5,6] respectively. Mechanical stability criteria are according to Ref. 7.[7] Bulk modulus (B) and shear modulus (G) are obtained from the arithmetic average of Voigt bound (subscript V) and Reuss bound (subscript R) as the Voigt-Reuss-Hill approximations.[8] It is known the Voigt bound is the upper limit of the actual effective moduli and is derived from the average polycrystalline moduli based on an assumption of uniform strain throughout a polycrystal, while the Reuss bound is obtained by assuming a uniform stress and is the lower limit of the actual effective moduli.[9] Both Voigt bound and Reuss bound are represented by the elastic stiffness constants C_{ij}.

Cubic phase (C_{11}, C_{44} and C_{12})

$$B_V = B_R = (C_{11} + 2C_{12})/3$$

$$G_V = (C_{11} – C_{12} + 3C_{44})/5$$

$$G_R = 5(C_{11} – C_{12})C_{44}/[4C_{44} + 3(C_{11}\text{-}C_{12})].$$

The mechanical stability criteria are given by

$$C_{11} > 0,\ C_{44} > 0,\ C_{11} > |C_{12}|,\ (C_{11} + 2C_{12}) > 0.$$

Hexagonal phase (C_{11}, C_{33}, C_{44}, C_{12}, and C_{13})

$$B_V = (1/9)[2(C_{11} + C_{12}) + 4C_{13}+C_{33}]$$

$$G_V = (1/30)(M + 12C_{44} + 12C_{66})$$

$$B_R = C^2/M$$

$$G_R = (5/2)[C^2C_{44}C_{66}]/[3B_VC_{44}C_{66} + C^2(C_{44} + C_{66})]$$

$$M = C_{11} + C_{12} +2C_{33} - 4C_{13}$$

$$C^2 = (C_{11} + C_{12})C_{33}\text{-}2C_{13}^2.$$

The mechanical stability criteria are given by

$$C_{44} > 0,\ C_{11} > |C_{12}|,\ (C_{11} + 2C_{12})C_{33}>2C_{13}^2.$$

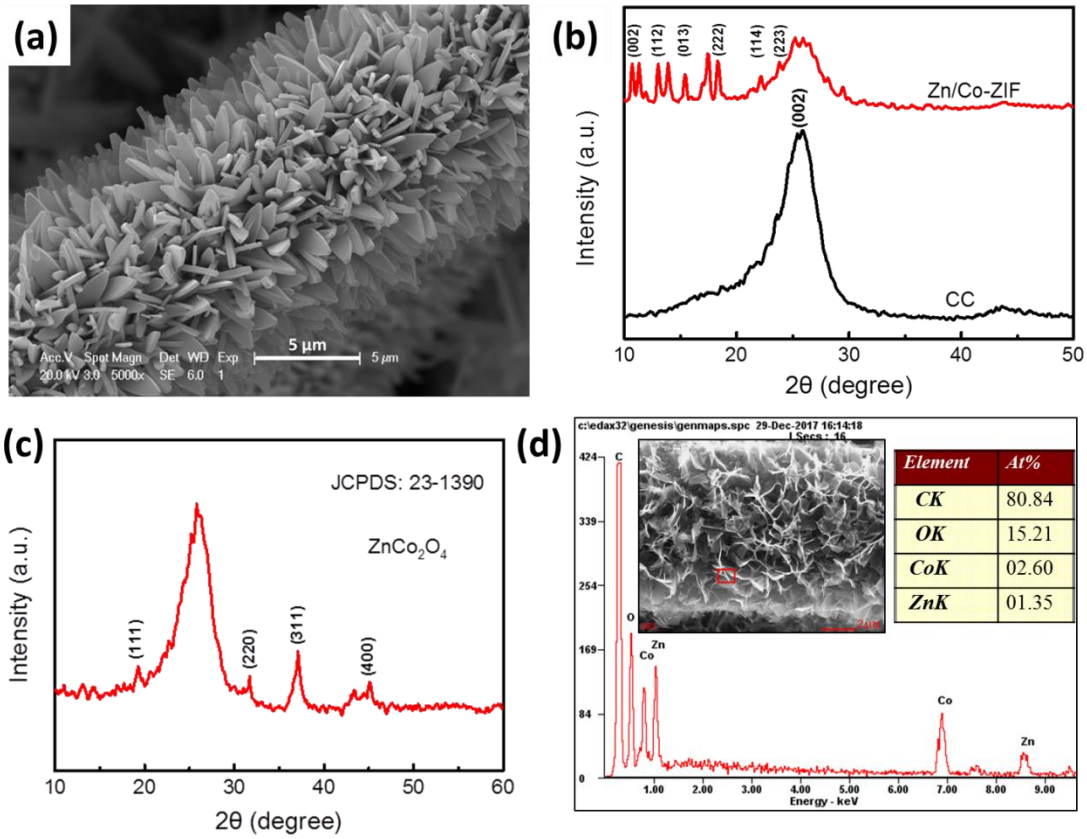

Fig. S1. (a) SEM image of monometallic Co-MOFs/CC, (b) XRD patterns of Zn/Co-based MOFs precursor and carbon cloth, (c) XRD pattern of ZnCoO-NSs, (d) the corresponding EDS spectrum of ZnCoO-NSs.

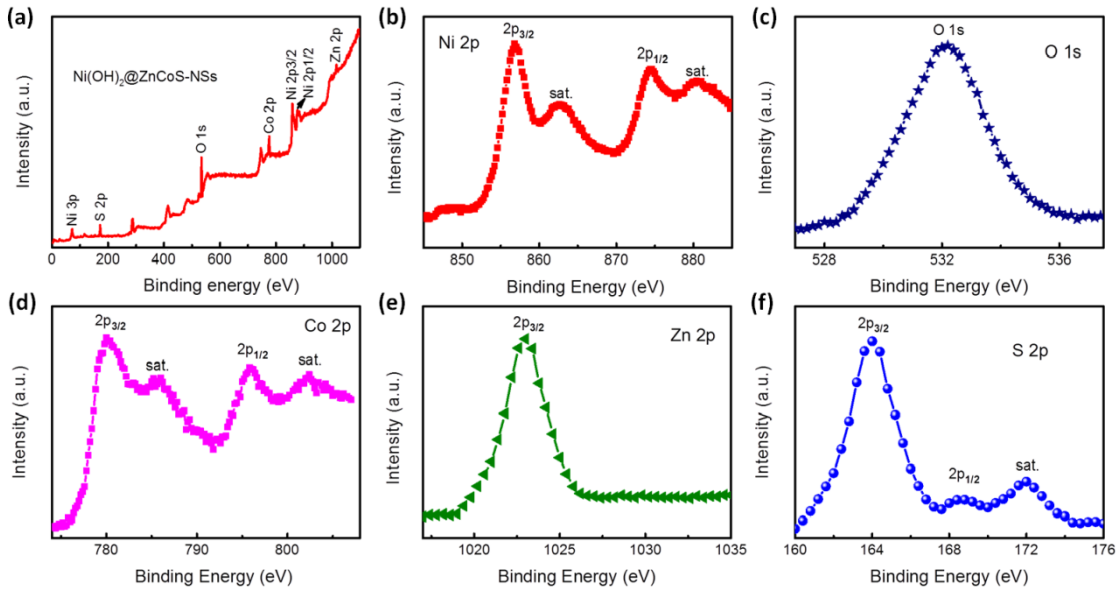

Fig. S2. XPS spectra of the $Ni(OH)_2$@ZnCoS-NSs: survey spectrum (a) and high-resolution spectra of Ni 2p (b), O 1s (c), Co 2p (d), Zn 2p (e), and S 2p (f).

The high-resolution spectra of Ni 2p and Co 2p (Figure S2b and d), they are well fitted with two kinds of spin-orbit doubles and two shakeup satellites (marked as "sat."). For Ni 2p spectrum, the two major peaks major peaks centered at binding energies of 856.1 and 874.4 eV correspond to the Ni $2p_{3/2}$ and Ni $2p_{1/2}$ signals of Ni^{2+} and Ni^{3+}, respectively. In the case of Co 2p spectrum, spin-orbit splitting values of Co $2p_{3/2}$ and Co $2p_{1/2}$ at 781.2 and 795.8 eV can be ascribed to Co^{2+} and Co^{3+}, respectively. The strong peak of Zn 2p (Figure S2e) located at 1023 eV corresponds to Zn $2p_{3/2}$ of the Zn(Ⅱ) oxidation state, which is the characteristic peak of Zn^{2+}. In addition, the peaks of O 1s and S 2p (Figure S2c and f) at 532 and 164.5 eV are originated from the metal-hydrogen-oxygen and sulfur-metal bonds, respectively, indicating the presence of $Ni(OH)_2$ and ZnCoS.

Table S1. Comparison of capacitances between our $Ni(OH)_2$@ZnCoS-NSs electrode and the Ni-Co oxides/hydroxides, mixed metal oxides/sulfides, and their corresponding hybrid structures electrode materials taken from the recently reported reports.

Electrode materials	Electrolyte	Maximum specific (areal) capacitance at current density	Year-Ref.
$Ni(OH)_2$-Mg/Ni foam	6 M KOH	1931 F g^{-1} at 0.5 A g^{-1}	2016[10]
$CoMoO_4$@Co_3O_4/OMEP	2 M KOH	7.13 F cm^{-2} (1168 F g^{-1}) at 4 mA cm^{-2}	2017[11]
$Ni(OH)_2$@$MnCo_2O_4$/Ni foam	2 M KOH	2154 F g^{-1} at 5 A g^{-1}	2016[12]
$Ni(OH)_2$@g-C_3N_4/Ni foam	6 M KOH	1768.7 F g^{-1} at 7 A g^{-1}	2017[13]
$MnMoO_4$@$NiCo_2O_4$/Ni foam	2 M KOH	1.91 F cm^{-2} (2010.5 F g^{-1}) at 1 mA cm^{-2}	2016[14]
$Ni(OH)_2$@FeOF/Ni foam	3 M KOH	1452 F g^{-1} at 1 A g^{-1}	2017[15]
MnO_2@$CoMoO_4$/GF	1 M KOH	8.01 F cm^{-2} (2666.7 F g^{-1}) at 3 mA cm^{-2}	2018[16]
Ni_3S_2@$CoNi_2S_4$/Ni foam	2 M KOH	2435 F g^{-1} at 2 A g^{-1}	2017[17]
$Ni(OH)_2$@Co_3O_4/Ni foam	3 M KOH	1306.3 F g^{-1} at 1.2 A g^{-1}	2017[18]
$Ni(OH)_2$@$NiCo_2O_4$/SiC NW	2 M KOH	3.12 F cm^{-2} (2580 F g^{-1}) at 4.8 mA cm^{-2}	2018[19]
$Ni(OH)_2$@H-TiO_2/CC	6 M KOH	1101.6 F g^{-1} at 1 mV s^{-1}	2017[20]
$Ni(OH)_2$@ZnCoS-NSs/CC	2 M KOH	8.1 F cm^{-2} (2730 F g^{-1}) at 3 mA cm^{-2}	This work

Note:

OMEP = 3D ordered macro-porous electrode palte

GF = graphene foam

NW = nanowires

CC = carbon cloth

NS = nanosheets

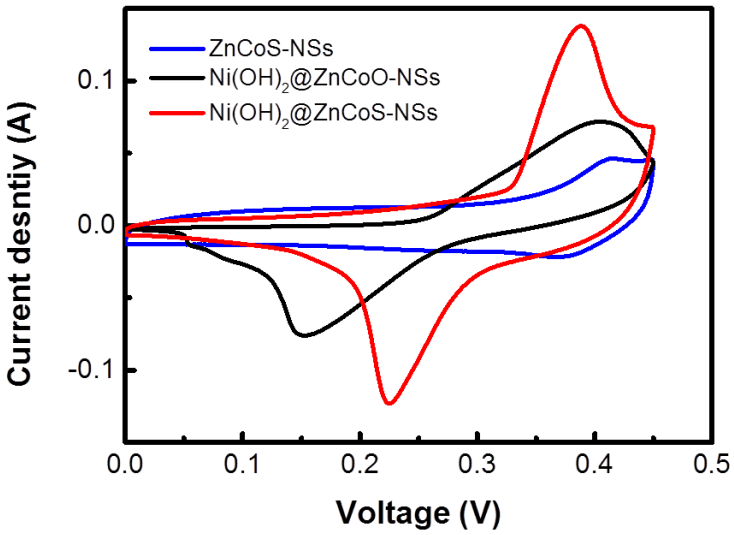

Fig. S3. Comparison of electrochemical performance of $Ni(OH)_2$@ZnCoS-NSs, $Ni(OH)_2$@ZnCoO-NSs, and ZnCoS-NSs electrodes: CV curves measured at a scan rate of 30 mV s^{-1}.

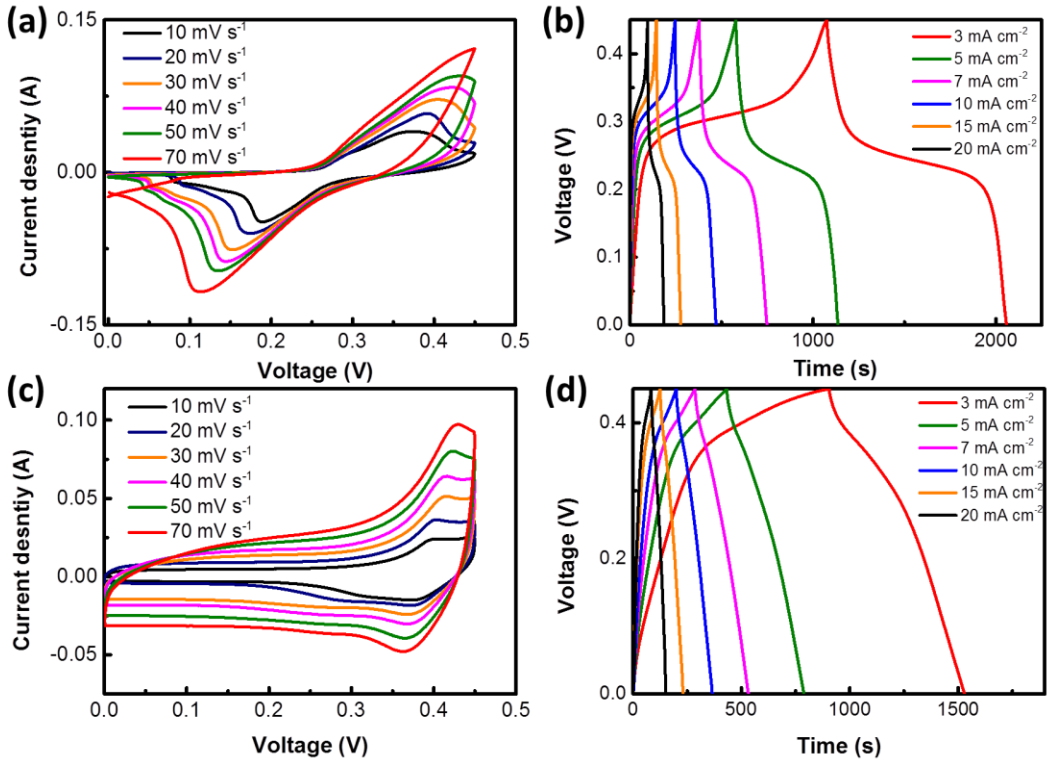

Fig. S4. CV curves and GCD curves of (a,b) $Ni(OH)_2$@ZnCoO-NSs and (c,d) ZnCoS-NSs electrodes collected at different scan rates and current densities.

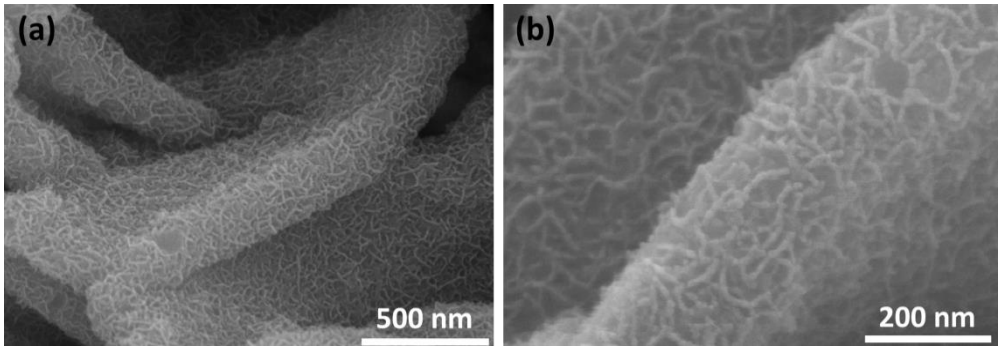

Fig. S5. SEM images of $Ni(OH)_2$@ZnCoS-NSs/CC electrode after 10000 cycling test.

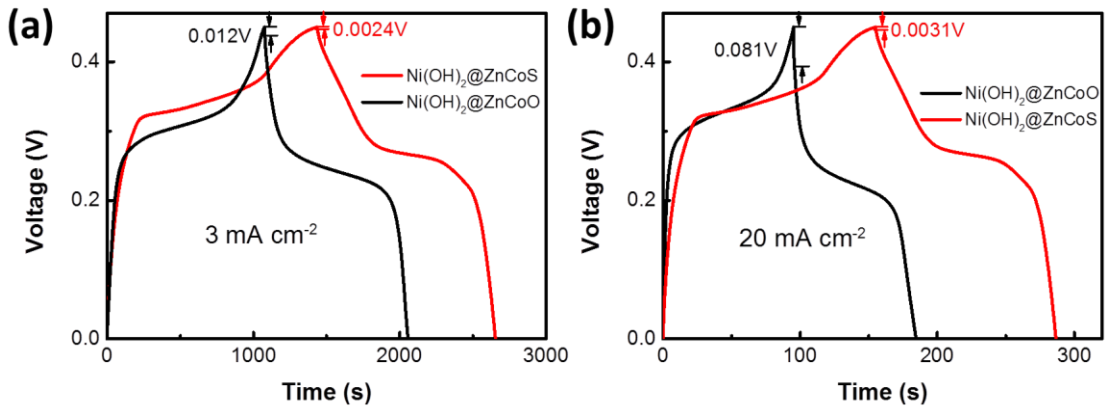

Fig. S6. Comparisons of the GCD curves of $Ni(OH)_2$@ZnCoO-NSs and $Ni(OH)_2$@ZnCoS-NSs at current densities of 1 and 5 mA cm^{-2}, respectively.

Table S2. Elastic stiffness constants C_{ij} (Gpa) for cubic ZnCoO, hexagonal ZnCoS and CoS.

Sample	C_{11}	C_{12}	C_{44}	C_{33}	C_{13}
ZnCoO	6803.72	2614.78	1622.60	~	~
CoS	3705.70	1691.29	890.74	3477.90	1528.41
ZnCoS	3153.12	1517.05	923.75	3639.41	1730.06

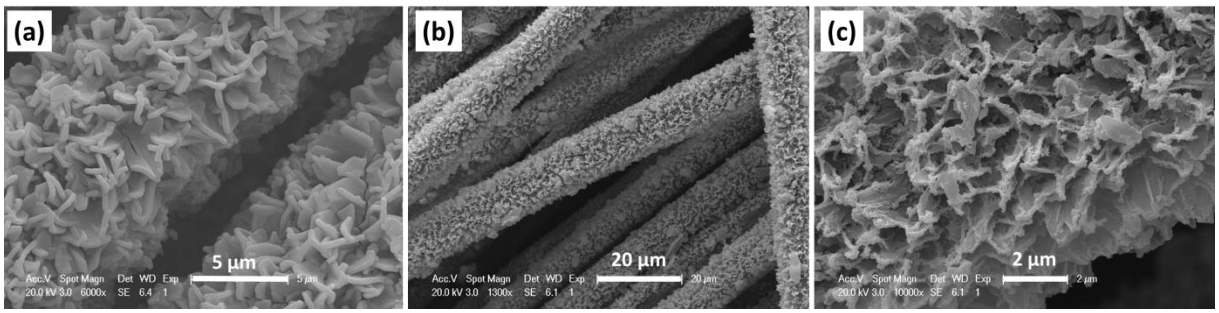

Fig. S7. SEM images of $Ni(OH)_2$@ZnCoO-NSs/CC electrode with the same mass of $Ni(OH)_2$ before (a) and after (b,c) 10000 cycling test.

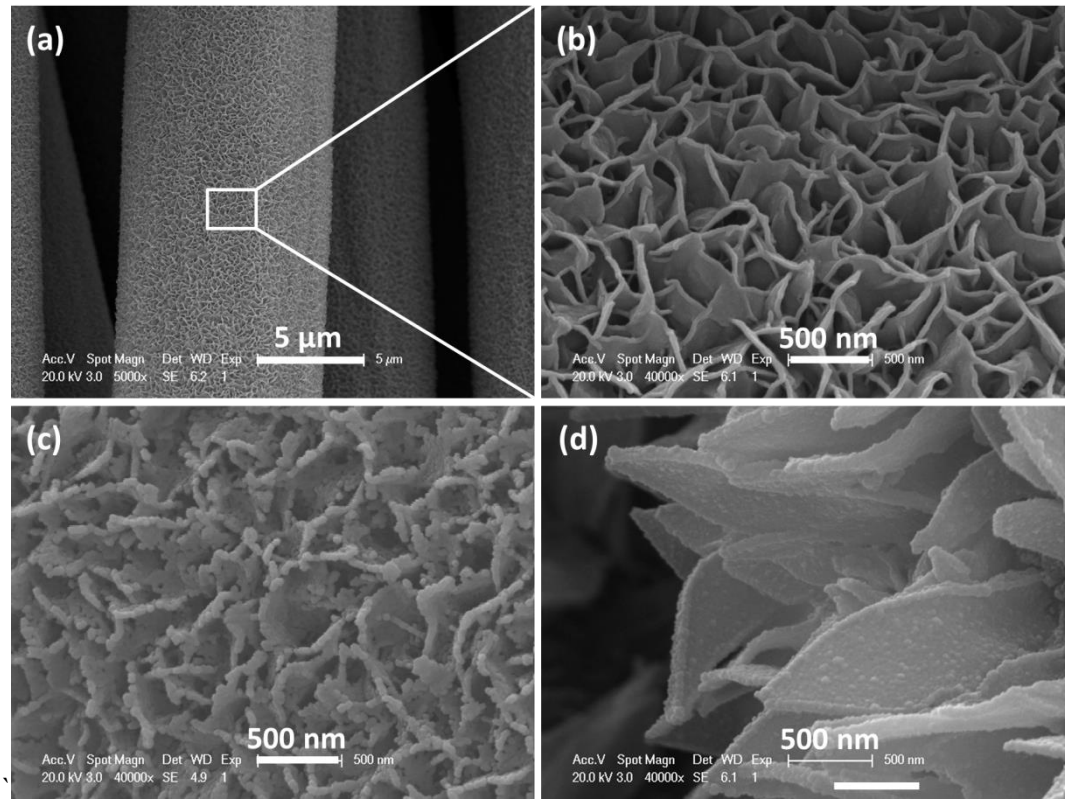

Fig. S8. (a) and (b) SEM images with different resolution of the unitary VN nanosheets covered on CC substrate before cycling test, (c) SEM image of the unitary VN nanosheets after 10000 cycling test, (d) SEM image of VN@ZnCoO-NSs electrode after 10000 cycling test.

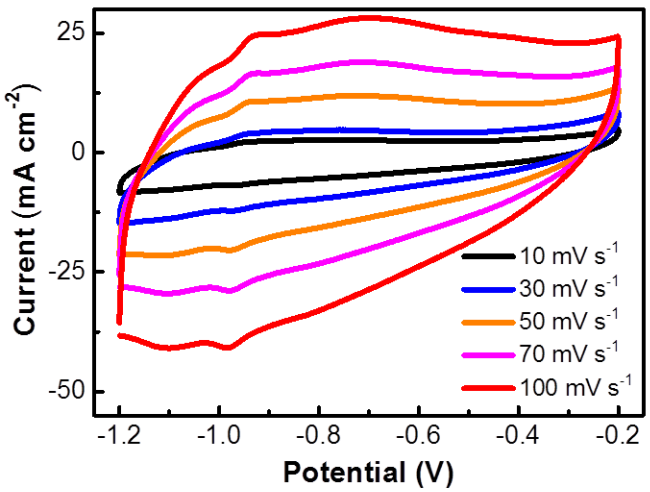

Fig. S9. CV curves of unitary VN nanosheets@CC electrode collected at different scan rates.

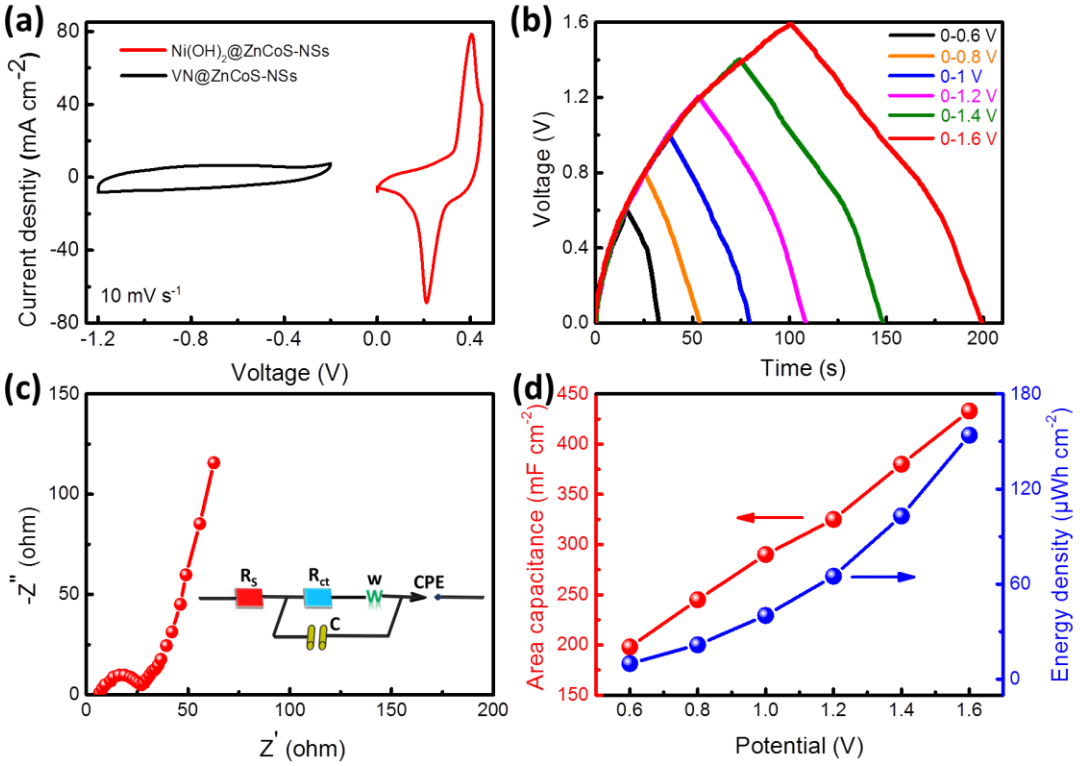

Fig. S10. (a) CV curves of the $Ni(OH)_2$@ZnCoS-NSs and VN@ZnCoS-NSs electrodes in separate potential windows at a scan rate of 10 mV s^{-1}, (b) GCD curves of the ASC device collected over different voltages from 0.6 to 1.6 V at a current density of 7 mA cm^{-2}, (d) Nyqusit plot of the ASC device, (d) area specific capacitance and energy density calculated based on GCD curves obtained at 7 mA cm^{-2}.

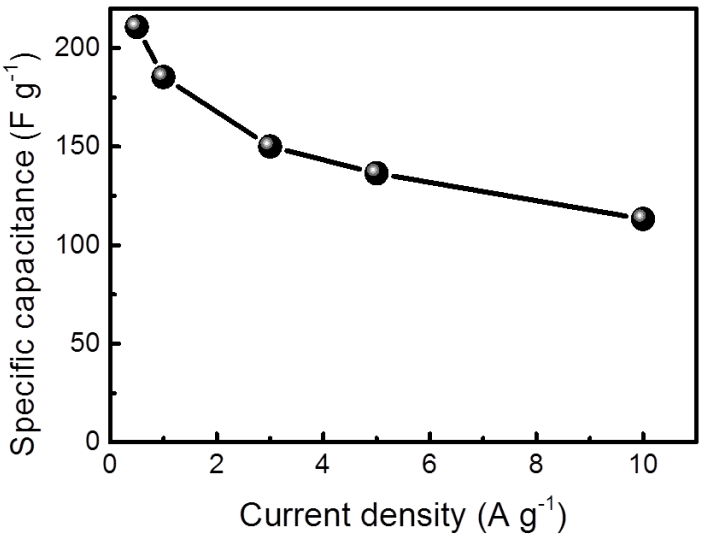

Fig. S11. Mass-specific capacitances of the $Ni(OH)_2$@ZnCoS-NSs//VN@ZnCoS-NSs ASC at different current densities.

Table S3. The maximum volume energy density comparison of our $Ni(OH)_2$@ZnCoS-NSs//VN@ZnCoS-NSs ASC with the reported quasi/all-solid-state supercapacitors.

ASC devices	Cell voltage (V)	electrolyte	Maximum energy density (mW h cm^{-3})	Reference
VO_x//VN	1.8	LiCI/PVA	0.61	21
H-TiO_2@MnO_2// H-TiO_2@C	1.8	LiCI/PVA	0.3	22
H-MnO_2//RGO	1.8	LiCI/PVA	0.25	23
$Ni(OH)_2$//OMC	1.5	KOH/PVA	2.16	24
Ni@NiO//RGO	1.5	KOH	1.06	25
Ti-Fe_2O_3@PEDOT //MnO_2	1.6	LiCI/PVA	0.89	26
MnO_x@Au-MSCs	0.8	H_2SO_4/PVA	1.75	27
Ni(OH)2@ZnCoS-N Ss//VN@ZnCoS-Ns	1.6	KOH/PVA	3.13	This work

Note:
RGO = reduced graphene oxide
OMC = ordered mesoporous carbon
PEDOT = ploy(3,4-ethylenedioxythiophene)
MSCs = micro-supercapacitors

References

1. G. Kresse and J. Furthmuller, *Computational Materials Science*, 1996, **6**, 15.
2. J. P. Perdew, K. Burke and M. Ernzerhof, *Phys. Rev. Lett.*, 1996, **77**, 3865.
3. P. E. Blochl, *Phys. Rev. B: Condens. Matter*, 1994, **50**, 17953.
4. G. Kresse and D. Joubert, *Phys. Rev. B*, 1999, **59**, 1758.
5. J. Haines, J. M. Leger and G. Bocquillon, *Ann Rev Mater Res*, 2001, **31**, 1.
6. J. P. Watt and L. Peselnick, *J Appl Phys*, 1980, **51**, 1525.
7. J. F. Nye, *Physical Properties of Crystals Oxford University Press*, Oxford, 1985.
8. R. Hill, Proc. *Phys. Soc. A*, 1952, **65**, 349.
9. Z. J. Wu, E. J. Zhao, H. P. Xiang, X. F. Hao, X. J. Liu and J. Meng, *Phys Rev B*, 2007, 76.
10. M. J. Xie, S. Y. Duan, Y. Shen, K. Fang, Y. Z. Wang, M. Lin and X. F. Guo, *ACS Energy Lett.*, 2016, **1**, 814.
11. M. Li, Y. Wang, H. Yang and P. K. Chu, *J. Mater. Chem. A*, 2017, **5**, 17312.
12. Y. Zhao, L. Hu, S. Zhao and L. Wu, *Adv. Funct. Mater.*, 2016, **26**, 4085.
13. B. Dong, M. Li, S. Chen, D. Ding, W. Wei, G. Gao and S. Ding, *ACS Appl. Mater. Interfaces*, 2017, **9**, 17890.
14. C. Y. Cui, J. T. Xu, L. Wang, D. Guo, M. L. Mao, J. M. Ma and T. H. Wang, *ACS Appl. Mater. Interfaces*, 2016, **8**, 8568.
15. M. Q. Wang, Z. Q. Li, C. X. Wang, R. Z. Zhao, C. X. Li, D. X. Guo, L. Y. Zhang and L. W. Yin, *Adv. Funct. Mater.*, 2017, **27**, 1701014.
16. S. Kumar, G. Saeed, N. H. Kim and J. H. Lee, *J. Mater. Chem. A*, 2018, **6**, 7182.
17. W. D. He, C. G. Wang, H. Q. Li, X. L. Deng, X. J. Xu and T. Y. Zhai, *Adv. Energy Mater.*,

2017, 7, 1700983.

18. X. Bai, Q. Liu, J. Liu, H. Zhang, Z. Li, X. Jing, P. Liu, J. Wang and R. Li, *Chem. Eng. J.*, 2017, **315**, 35.
19. J. Zhao, Z. J. Li, X. C. Yuan, Z. Yang, M. Zhang, A. Meng and Q. D. Li, *Adv. Energy Mater.*, 2018, **8**, 1702787.
20. Q. Q. Ke, C. Guan, X. Zhang, M. Zheng, Y. W. Zhang, Y. Q. Cai, H. Zhang and J. Wang, *Adv. Mater.*, 2017, **29**, 1604164.
21. X. H. Lu, M. H. Yu, T. Zhai, G. M. Wang, S. L. Xie, T. Y. Liu, C. L. Liang, Y. X. Tong and Y. Li, *Nano Lett.*, 2013, **13**, 2628.
22. X. H. Lu, M. H. Yu, G. M. Wang, T. Zhai, S. L. Xie, Y. C. Ling, Y. X. Tong and Y. Li, *Adv. Mater.*, 2013, **25**, 267.
23. T. Zhai, S. Xie, M. Yua, P. Fang, C. Liang, X. Lu and Y. Tong, *Nano Energy*, 2014, **8**, 255.
24. X. Dong, Z. Guo, Y. Song, M. Hou, J. Wang, Y. Wang and Y. Xia, *Adv. Funct. Mater.*, 2014, **24**, 3405.
25. M. Yu, W. Wang, C. Li, T. Zhai, X. Lu and Y. Tong, *NPG Asia Materials*, 2014, **6**, e129.
26. Y. Zeng, Y. Han, Y. Zhao, Y. Zeng, M. Yu, Y. Liu, H. Tang, Y. Tong and X. Lu, *Adv. Energy Mater.*, 2015, **5**, 1402176.
27. W. P. Si, C. L. Yan, Y. Chen, S. Oswald, L. Y. Hana and O. G. Schmidtabde, *Energy Environ. Sci.*, 2013, **6**, 3218